PROCEEDINGS OF SCIENCE

Investigating thermalization of a strongly interacting non-Abelian plasma

Loredana Bellantuono
Institute of Physics, Jagiellonian University, Lojasiewicza 11, 30-348 Krakow, Poland
E-mail: loredana.bellantuono@ba.infn.it

Pietro Colangelo
Istituto Nazionale di Fisica Nucleare - Sezione di Bari, via Orabona 4, 70125 Bari, Italy
E-mail: pietro.colangelo@ba.infn.it

Fulvia De Fazio*
Istituto Nazionale di Fisica Nucleare - Sezione di Bari, Italy
E-mail: fulvia.defazio@ba.infn.it

Floriana Giannuzzi
Istituto Nazionale di Fisica Nucleare - Sezione di Bari, Italy
E-mail: floriana.giannuzzi@ba.infn.it

Stefano Nicotri
Istituto Nazionale di Fisica Nucleare - Sezione di Bari, Italy
E-mail: stefano.nicotri@ba.infn.it

Using gauge/gravity duality methods, we study the relaxation towards equilibrium of strongly interacting non-Abelian matter. We adopt boundary sourcing to drive the system out-of-equilibrium, and analyze the equilibration process through local probes (energy density and pressures) and nonlocal probes (lengths of the geodesics between two boundary points and extremal surfaces having a Wilson loop as contour on the boundary). We also investigate the real-time dissociation of the heavy quarkonium in the out-of-equilibrium plasma. Systematic comparison with the results of a geometry dual to viscous hydrodynamics sheds light on the thermalization process.

EPS-HEP 2017, European Physical Society conference on High Energy Physics
5-12 July 2017
Venice, Italy

*Speaker.

© Copyright owned by the author(s) under the terms of the Creative Commons Attribution-NonCommercial-NoDerivatives 4.0 International License (CC BY-NC-ND 4.0).

PoS(EPS-HEP2017)541

1. Introduction

Within an elapsed time of $\mathscr{O}(1\,\mathrm{fm})$ the strongly interacting matter produced in relativistic heavy ion collisions evolves from the far-from-equilibrium state to a viscous hydrodynamic regime [1]. The description of the pre-equilibrium configuration and of the transition to the hydrodynamic behavior is an issue difficult to face theoretically [2]. Suitable methods make use of the gauge/gravity duality approach, invoking a correspondence between a strongly coupled conformal field theory on a 4D Minkowski space $\mathscr{M}_4$, and a weakly coupled gravity theory on $\mathrm{AdS}_5\times\mathrm{S}_5$, the *bulk*, of which $\mathscr{M}_4$ is the boundary [3–5]. Thermalization in the boundary theory corresponds to the formation of a black-hole in the bulk with time-dependent horizon, and it can be probed considering the boundary theory stress-energy tensor $T_{\mu\nu}$, as well as correlation functions of boundary theory operators.

Among the 4D coordinates $x^\mu = (x^0, x^1, x^2, x^3)$, we identify $x^3 = x_\parallel$ with the collision axis. Writing $x^0 = \tau\cosh y$ and $x^3 = \tau\sinh y$ in terms of proper time τ and rapidity y, the Minkowski metric reads: $ds^2 = -d\tau^2 + \tau^2 dy^2 + dx_\perp^2$, with $x_\perp = \{x^1, x^2\}$. Boost-invariance along $x_\parallel$, rotation and translation invariance in the $x_\perp$ plane imply for an expanding inviscid fluid that $T_{\mu\nu}$ is diagonal, with components (energy density, transverse and longitudinal pressures) depending only on τ: $\varepsilon(\tau) = \dfrac{c}{\tau^{4/3}}$ and $p_\parallel = -\varepsilon(\tau) - \tau\varepsilon'(\tau)$, $p_\perp = \varepsilon(\tau) + \tau\varepsilon'(\tau)/2$, with c a constant [6]. Corrections for viscous hydrodynamics modify these relations:

$$\varepsilon(\tau) = \frac{3\pi^4\Lambda^4}{4(\Lambda\tau)^{4/3}}\left[1 - \frac{2c_1}{(\Lambda\tau)^{2/3}} + \frac{c_2}{(\Lambda\tau)^{4/3}} + \mathscr{O}\left(\frac{1}{(\Lambda\tau)^2}\right)\right] \tag{1.1}$$

$$p_\parallel(\tau) = \frac{\pi^4\Lambda^4}{4(\Lambda\tau)^{4/3}}\left[1 - \frac{6c_1}{(\Lambda\tau)^{2/3}} + \frac{5c_2}{(\Lambda\tau)^{4/3}} + \mathscr{O}\left(\frac{1}{(\Lambda\tau)^2}\right)\right] \tag{1.2}$$

$$p_\perp(\tau) = \frac{\pi^4\Lambda^4}{4(\Lambda\tau)^{4/3}}\left[1 - \frac{c_2}{(\Lambda\tau)^{4/3}} + \mathscr{O}\left(\frac{1}{(\Lambda\tau)^2}\right)\right] , \tag{1.3}$$

with $c_{1,2}$ numerical constants and Λ a parameter [7]. An effective fluid temperature can be defined: $\varepsilon(\tau) = \frac{3}{4}\pi^4 T_{eff}(\tau)^4$. Invoking the gauge/gravity correspondence, the dual of $T_{\mu\nu}$ is the 5D metric tensor g_{MN}, hence modifications of the bulk geometry produce variations in $T_{\mu\nu}$, which can be determined through a near-boundary expansion of g_{MN} [8].

To implement effects driving the boundary system out-of-equilibrium, a distortion (a *quench*) in the 4D metric can be introduced with profile $\gamma(\tau)$ [9], writing the boundary line element as $ds^2 = -d\tau^2 + e^{\gamma(\tau)}dx_\perp^2 + \tau^2 e^{-2\gamma(\tau)}dy^2$. The corresponding 5D metric can be expressed using Eddington-Finkelstein coordinates, introducing the fifth radial coordinate r so that the boundary is reached for $r\to\infty$: $ds^2 = 2drd\tau - Ad\tau^2 + \Sigma^2 e^B dx_\perp^2 + \Sigma^2 e^{-2B}dy^2$. The metric functions A, Σ, B depend on r and τ only, due to the imposed symmetries. They can be computed solving the Einstein equations with the constraint that the 4D metric with quench is recovered for $r\to\infty$. Moreover, switching the quench on at $\tau = \tau_i$, the metric functions must reproduce the AdS_5 geometry at τ_i. A suitable expression for such equations has been worked out in [9], and an efficient solution algorithm developed in [10] has been applied to different quench profiles $\gamma(\tau)$. The equilibration time can be determined comparing the behavior of the various observables with the corresponding hydrodynamic quantities. Here we describe the results for two profiles, denoted as model $\mathscr{A}_2$ and model $\mathscr{B}$, which represent two different kinds of impulsive distortion of the boundary geometry.

PoS(EPS-HEP2017)541

2. Role of local versus nonlocal observables to probe thermalization

The quench profiles for model $\mathscr{A}_2$ and model $\mathscr{B}$ are depicted in the top panels of Fig. 1. The deformation persists up to $\tau_f^{\mathscr{A}} = 3.25$ in model $\mathscr{A}_2$, and up to $\tau_f^{\mathscr{B}} = 5$ in model $\mathscr{B}$. The lower panels in the figure display the $T_{\mu\nu}$ components [10]. To investigate the late time behavior, Fig. 2 shows the components of $T_{\mu\nu}$ after the end of the quench in comparison with Eqs. (1.1)-(1.3). $\varepsilon(\tau)$ follows the viscous hydrodynamics behavior right after the end of the quenches, while a pressure anisotropy persists up to $t_{isotr}^{\mathscr{A}} = 6$ and $t_{isotr}^{\mathscr{B}} = 6.74$ [10]. Imposing that at the end of the quench the temperature is $T_{eff} = 500$ MeV, the thermalization times turn out to be of $\mathscr{O}(1\text{ fm})$.

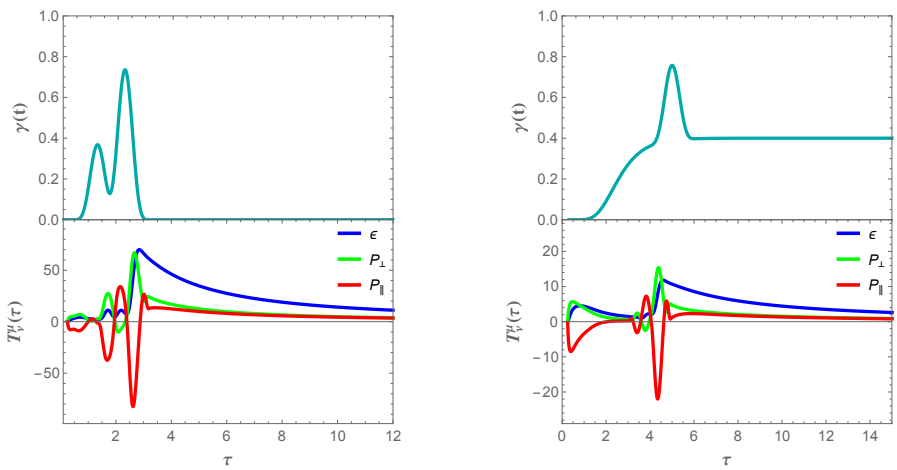

Figure 1: Profile $\gamma(\tau)$ (upper panel) and components of T_ν^μ for the quench model $\mathscr{A}_2$ (left) and $\mathscr{B}$ (right).

The components of $T_{\mu\nu}$ are local observables mainly sensitive to the geometry close to the boundary. In the holographic approach one can also access nonlocal probes, namely the two-point correlation function of boundary theory operators, and the expectation values of Wilson loops on the boundary. This requires the calculation of the length of the geodesics in the bulk connecting the two boundary points in the correlation function, or the area of the extremal surface plunging in the bulk and having the Wilson loop as contour at the boundary [11]. They have been computed for models $\mathscr{A}_2$ and $\mathscr{B}$ and compared to the corresponding quantities in viscous hydrodynamics [12]. The 5D metric reproducing the results (1.1)-(1.3) has been worked out in [12, 13].

The length of a curve connecting the points P, Q on the boundary is $\mathscr{L} = \int_P^Q d\lambda \sqrt{\pm g_{MN}\dot{x}^M\dot{x}^N}$, where the coordinates $x^M(\lambda)$ depend on the parameter λ, and $\dot{x}^M \equiv dx^M/d\lambda$ [14, 15]. Viewing the integrand in $\mathscr{L}$ as a Lagrangian and solving the corresponding Euler-Lagrange equations, the geodesic can be determined. In the Eddington-Finkelstein coordinates, the space-like path connecting the boundary points $P = (t_0, -\ell/2, x_2, y)$ and $Q = (t_0, \ell/2, x_2, y)$ that extends in the bulk at fixed (x_2, y) is described by the functions $\tau(x)$ and $r(x)$, with $x_1 \equiv x$, and $\tau(0) = \tau_*$, $r(0) = r_*$, $\tau'(0) = r'(0) = 0$. Boundary conditions are $\tau(-\ell/2) = \tau(\ell/2) = t_0$, $r(-\ell/2) = r(\ell/2) = r_0$. In the calculation r_0 is set to $r_0 = 12$. The result for the geodesic length is $\mathscr{L} = \int_{-\ell/2}^{\ell/2} dx \frac{\tilde{\Sigma}(r,\tau)}{\sqrt{\tilde{\Sigma}(r_*,\tau_*)}}$ with $\tilde{\Sigma}(r,\tau) \equiv \Sigma(r,\tau)^2 e^{B(r,\tau)}$ computed in correspondence to the solution $(r(x), \tau(x))$. The calculation

PoS(EPS-HEP2017)541

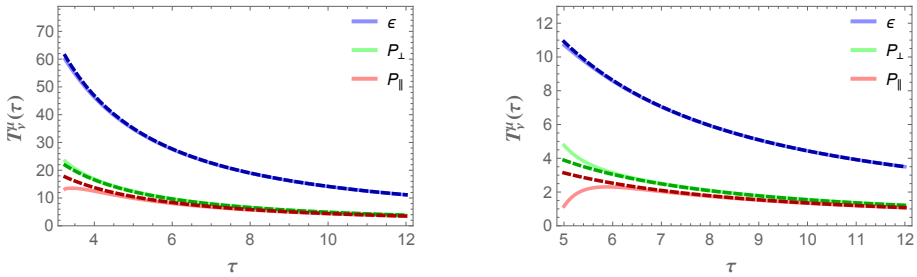

Figure 2: $\varepsilon(\tau)$, $p_\perp(\tau)$ and $p_\parallel(\tau)$ computed in model $\mathscr{A}_2$ for $\tau > \tau_f^{\mathscr{A}}$ (left) and in model $\mathscr{B}$ for $\tau > \tau_f^{\mathscr{B}}$ (right). The dashed lines correspond to the viscous hydrodynamic expressions (1.1)-(1.3).

for Wilson loops is described in [12], where two different shapes have been considered, a circle (C) and an infinite rectangular strip (R). Fig. 3 displays for models $\mathscr{A}_2$ and $\mathscr{B}$ the differences $\Delta\mathscr{L}$, ΔA_R and ΔA_C between each one of these three geometrical quantities and the corresponding quantity computed in the hydrodynamic setup, after the end of the quenches. The thermalization time, when the differences vanish, increases with the size of the probe, a feature of strongly coupled systems. To compare to the results from local probes, fig. 4 shows $\Delta\mathscr{L}$, ΔA_R, ΔA_C versus ℓ in model

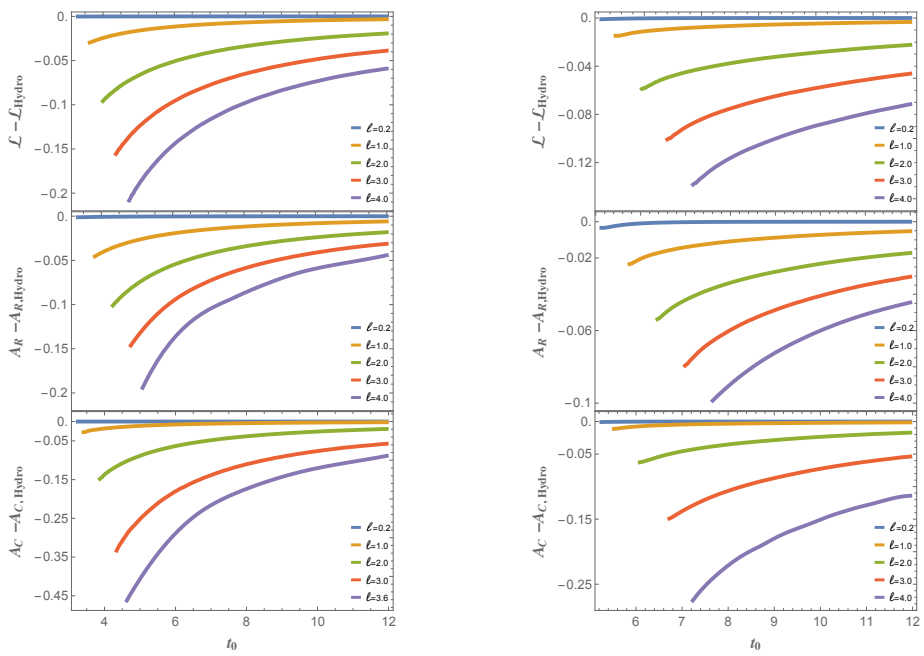

Figure 3: Results for model $\mathscr{A}_{(2)}$ (left) and $\mathscr{B}$ (right): difference between the geodesic length (top panel), the area of the extremal surface for the rectangular Wilson loop (middle), and for the circular Wilson loop (bottom) in the models with quench and with the hydrodynamic metric. t_0 starts after the end of the quench.

PoS(EPS-HEP2017)541

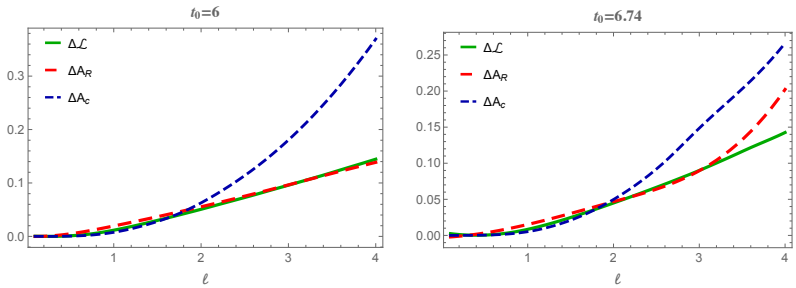

Figure 4: Differences $\Delta\mathscr{L}$, ΔA_R, ΔA_C in model $\mathscr{A}_2$ at $t_0 = 6$ (left), and in model $\mathscr{B}$ at $t_0 = 6.74$ (right) versus the size of the probe.

$\mathscr{A}_2$ at $t_0 = t^{\mathscr{A}}_{isotr} = 6$ and in model $\mathscr{B}$ at $t_0 = t^{\mathscr{B}}_{isotr} = 6.74$: only for small ℓ the differences are zero.

3. Real-time quarkonium dissociation in the far-from-equilibrium medium

In the holographic approach quarks are dual to open strings in the bulk [16]. In [17] the real-time evolution of a string extending between two endpoints, representing a heavy quark and an antiquark, kept close to the boundary, is studied. The strings falls down under gravity and, at finite temperature, it can reach the black-hole horizon, an event interpreted as the in-medium quarkonium dissociation [18, 19]. The string dynamics is governed by Nambu-Goto action $S_{NG} = -T_f \int d\tau d\sigma \sqrt{-g}$, with $T_f = \dfrac{1}{2\pi\alpha'}$, $\alpha' = \frac{R_5^2}{\sqrt{\lambda}}$, R_5 the AdS$_5$ radius and λ the 't Hooft coupling. g is the determinant of the induced world-sheet metric, and (τ, σ) the world-sheet coordinates. We consider strings in a 3D slice of the bulk described by the coordinates (t, w, r), with two choices for w. The first one is $w = x$, with $x = x_1$ or $x = x_2$, and the string endpoints kept fixed at mutual distance $2L$ close to the boundary. The second one is $w = y$ along the rapidity axis, representing a quark and an antiquark moving away from each other in the longitudinal direction $x_\parallel$ with rapidity y_L. Choosing $\tau = t$ and $\sigma = w$, the string profile is a function $r(t, w)$. In terms of the metric functions A, B, Σ, we find $S_{NG} = -T_f \int dt\, dw \sqrt{\Sigma_w(t,r)\,(A(t,r) - 2\,\partial_t r) + (\partial_w r)^2}$, where $\Sigma_w = \bar{\Sigma} = \Sigma^2 e^{-2B}$ if $w = y$ and $\Sigma_w = \tilde{\Sigma} = \Sigma^2 e^{B}$ if $w = x$. The resulting equation of motion for $r(t,w)$ is ($r' = dr/dw$):

$$r'' - \frac{\partial_w g}{2g} r' + \frac{\partial_t g}{2g}\Sigma_w - \partial_t \Sigma_w + \frac{\partial_r g}{2} = 0\,. \tag{3.1}$$

Since the metric is time-dependent, the solution depends on the initial time t_i when the string is completely stretched close to the boundary: $r(t_i, w) = r_{max}$ for all w (we set $r_{max} = 12$). The string endpoints are kept fixed at $w_Q = -L$ and $w_{\overline{Q}} = L$ in the $w = x$ case, and $w_Q = -y_L$ and $w_{\overline{Q}} = y_L$ for the $w = y$ configuration, so that $r(t, w_{\overline{Q}}) = r(t, w_Q) = r_{max}$. We vary L and y_L in the range $[0.1, 100]$ and impose the initial velocity $\dot{r}(t_i, w) = v$, with $v = 0, -0.5, -1$. Fig. 5 displays the string profile in model $\mathscr{B}$ for $w = x$ and $L = 0.1$. Similar profiles are found for $w = y$ and in model $\mathscr{A}_{(2)}$. The dissociation time t_D (finite in the chosen coordinate system) is determined when the string reaches the horizon. Fig. 6 shows t_D versus t_i in the two models. In each column, the upper panel displays t_D for the $w = y$ configuration with $y_L = 10$, and the bottom panel refers to t_D in the $w = x$ configuration with $L = 10$. After the end of the quenches, t_D varies smoothly

PoS(EPS-HEP2017)541

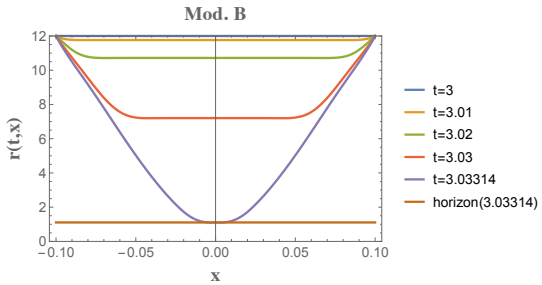

Figure 5: String profile $r(t,w)$, corresponding to $\{t_i, v, L\} = \{3, -1, 0.1\}$, for the transverse $w = x$ configuration and quench model $\mathscr{B}$ as a function of x at different t, until the horizon is reached.

and approaches values close to each other in the two models. During the quenches, t_D abruptly fluctuates with a different behavior for the two string configurations, similarly to the pressures $p_{\|}$ and $p_{\perp}$ [10] and to the screening length [20]. Fig. 7 compares the result for t_D in model $\mathscr{B}$ and in viscous hydrodynamics. The hydrodynamic behavior is recovered right after the end of the quench, and t_D asympotically approaches the time required to reach the AdS center starting from $r = r_{max}$: $t_\infty = \frac{2}{3r_{max}} {}_2F_1\left(1, \frac{5}{4}, \frac{7}{4}, -1\right)$.

4. Conclusions

Holographic methods allow us to describe the thermalization of a strongly interacting non-Abelian plasma, driven out-of-equilibrium by a quench on the boundary geometry. Local and nonlocal observables provide indications on the thermalization time at various length scales. The energy density follows the hydrodynamic viscous behavior after the end of the quench, while the pressures take longer. For nonlocal observables the thermalization time increases with the size

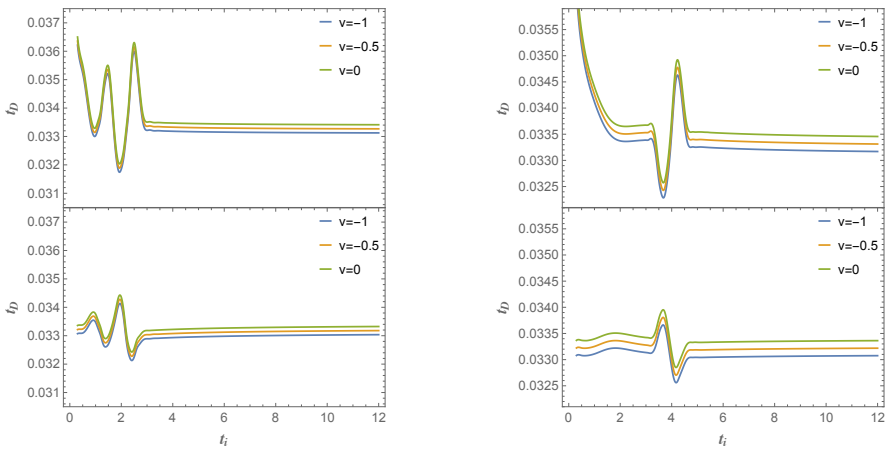

Figure 6: t_D versus t_i in model $\mathscr{A}_{(2)}$ (left) and $\mathscr{B}$ (right). Top panels: $w = y$ string configuration with $y_L = 10$. Bottom panels: $w = x$ configuration with $L = 10$.

PoS(EPS-HEP2017)541

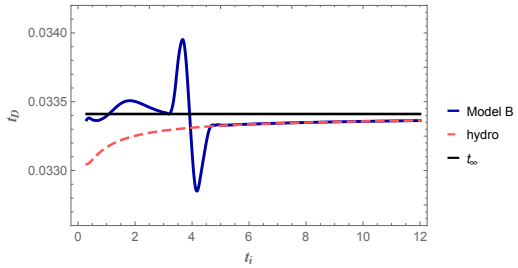

Figure 7: t_D versus t_i for $w = x$, $L = 10$ and $v = 0$, for quench model $\mathscr{B}$ (continuous line) and for a geometry dual to viscous hydrodynamics (dashed line). The horizontal line corresponds to the asymptotic value t_∞.

of the probe. Quarkonium dissociation is a fast phenomenon: the dissociation time follows the behavior of viscous hydrodynamics as soon as the quench is switched off.

These studies have been carried out within the INFN project QFT-HEP. LB thanks the Angelo Della Riccia Foundation for financial support.

References

[1] P. Braun-Munzinger *et al.*, *Phys. Rept.* **621** (2016) 76.

[2] See, e.g., M. Ruggieri, L. Oliva, G. X. Peng and V. Greco, arXiv:1707.07956 [nucl-th] and references therein.

[3] J. M. Maldacena, *Int.J.Theor.Phys.* **38** (1999) 1113.

[4] E. Witten, *Adv.Theor.Math.Phys.* **2** (1998) 253.

[5] S. Gubser, I. R. Klebanov and A. M. Polyakov, *Phys.Lett.* **B428** (1998) 105.

[6] J. Bjorken, *Phys.Rev.* **D27** (1983) 140.

[7] R. A. Janik and R. B. Peschanski, *Phys. Rev.* **D73** (2006) 045013.

[8] S. de Haro *et al.*, *Commun.Math.Phys.* **217** (2001) 595.

[9] P. M. Chesler and L. G. Yaffe, *Phys. Rev. Lett.* **102** (2009) 211601.

[10] L. Bellantuono, P. Colangelo, F. De Fazio and F. Giannuzzi, *JHEP* **07** (2015) 053.

[11] V. Balasubramanian et al., *Phys. Rev. Lett.* **106** (2011) 191601.

[12] L. Bellantuono, P. Colangelo, F. De Fazio, F. Giannuzzi and S. Nicotri, *Phys. Rev.* **D94** (2016) 025005.

[13] W. van der Schee, *Phys. Rev.* **D87** (2013) 061901.

[14] V. Balasubramanian and S. F. Ross, *Phys. Rev.* **D61** (2000) 044007.

[15] J. Louko, D. Marolf and S. F. Ross, *Phys. Rev.* **D62** (2000) 044041.

[16] A. Karch and E. Katz, *JHEP* **06** (2002) 043.

[17] L. Bellantuono, P. Colangelo, F. De Fazio, F. Giannuzzi and S. Nicotri, *Phys. Rev.* **D96** (2017) 034031.

[18] S. Lin and E. Shuryak, *Phys. Rev.* **D77** (2008) 085013.

[19] I. Iatrakis and D. E. Kharzeev, *Phys. Rev.* **D93** (2016) 086009].

[20] H. Liu, K. Rajagopal and U. A. Wiedemann, *Phys. Rev. Lett.* **98** (2007) 182301.

PoS(EPS-HEP2017)541